Supporting Information

Wet-Chemical Assembly of 2D Nanomaterials into Lightweight, Microtube-Shaped, and Macroscopic 3D Networks

Florian Rasch[1], Fabian Schütt[1], Lena M. Saure[1,2], Sören Kaps[1], Julian Strobel[3], Oleksandr Polonskyi[4], Ali Shaygan Nia[5], Martin R. Lohe[5], Yogendra K. Mishra[6], Franz Faupel[4], Lorenz Kienle[3], Xinliang Feng[5], Rainer Adelung[1]*

[1]*Chair for Functional Nanomaterials, Institute for Materials Science, Kiel University, Kaiserstr. 2, 24143 Kiel, Germany*

[2]*Chair of Engineering Mechanics, Brandenburg University of Technology Cottbus-Senftenberg, Großenhainer Straße 57, 01968 Senftenberg, Germany*

[3]*Chair for Synthesis and Real Structure, Institute for Materials Science, Kiel University, Kaiserstr. 2, 24143 Kiel, Germany*

[4]*Chair for Multicomponent Materials, Institute for Materials Science, Kiel University, Kaiserstr. 2, 24143 Kiel, Germany*

[5]*Department of Chemistry and Food Chemistry, Center for Advancing Electronics Dresden (cfaed), Technische Universität Dresden, 01062 Dresden, Germany*

[6]*NanoSYD, Mads Clausen Institute, University of Southern Denmark, Alsion 2, DK-6400 Sønderborg, Denmark*

E-mail:
fas@tf.uni-kiel.de

Figure S1

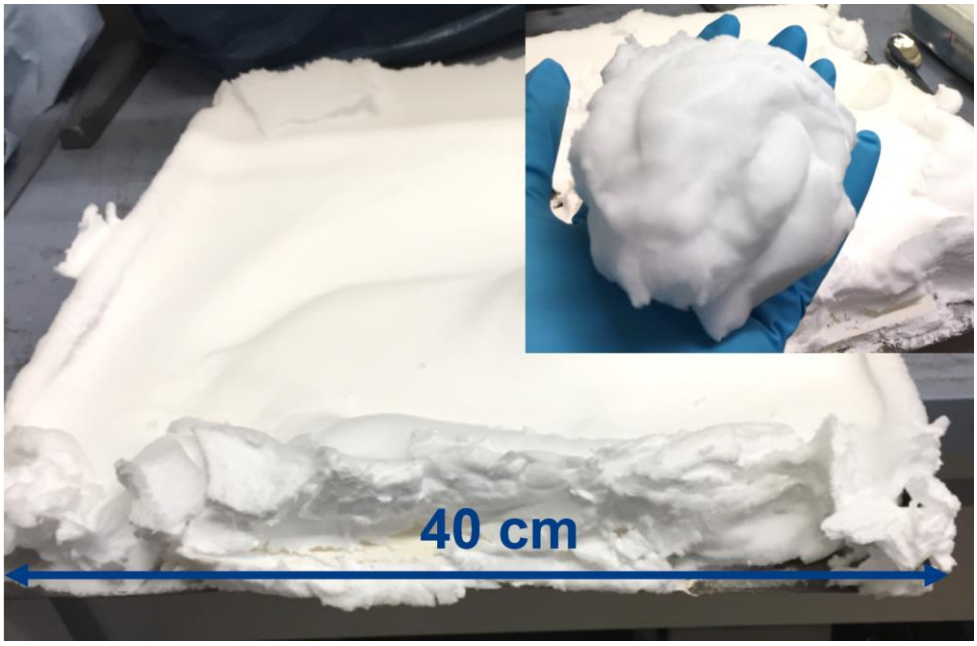

Figure S1. Upscaled synthesis of t-ZnO powder in collaboration with Phi-Stone AG.

Figure S2

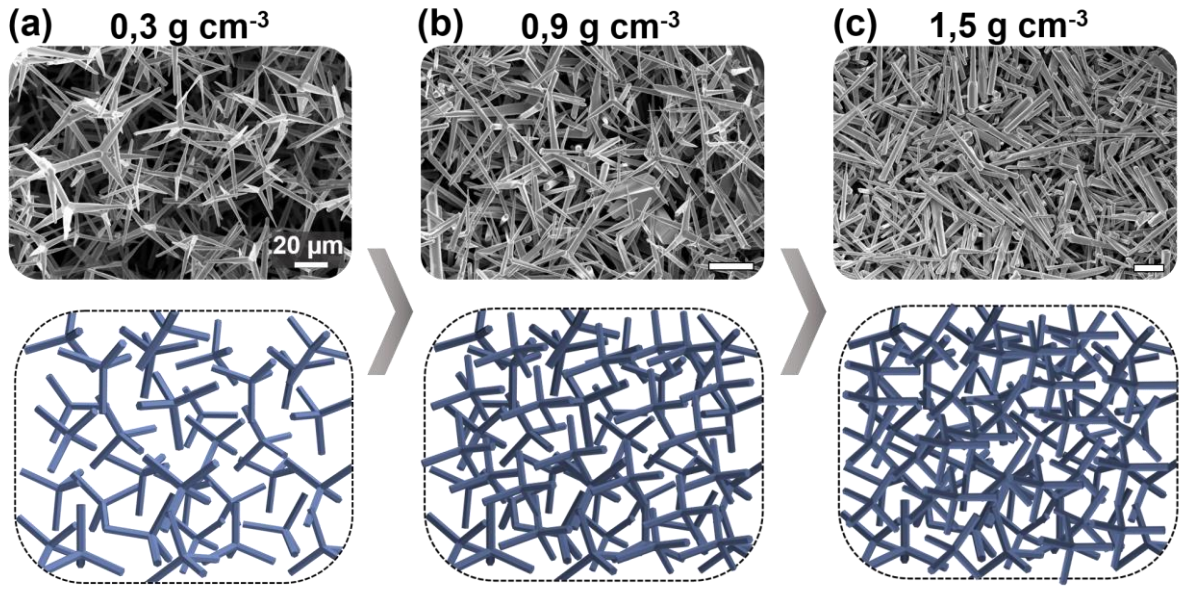

Figure S2. Tunable template density: Representative SEM images and corresponding schematics of ZnO networks with increasing density from **a)-c)**, illustrating the adjustable porosity of the templates.

Figure S3

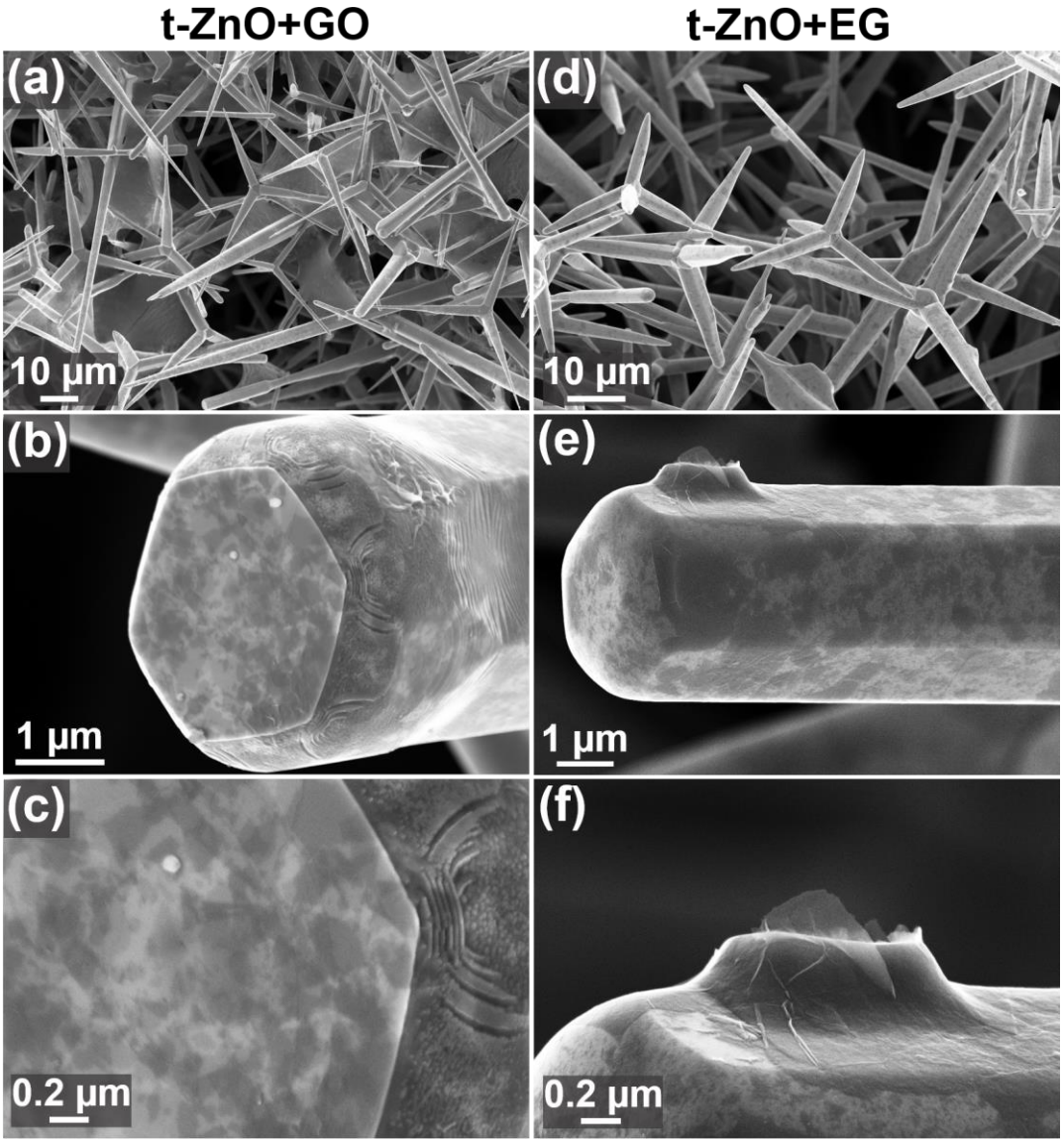

Figure S3. Wet-chemical assembly of 2D carbon nanomaterials on ceramic template: SEM images with increasing magnification (from top to bottom) of macroscopic t-ZnO network coated with **a)-c)** GO sheets or **d)-f)** EG sheets.

Figure S4

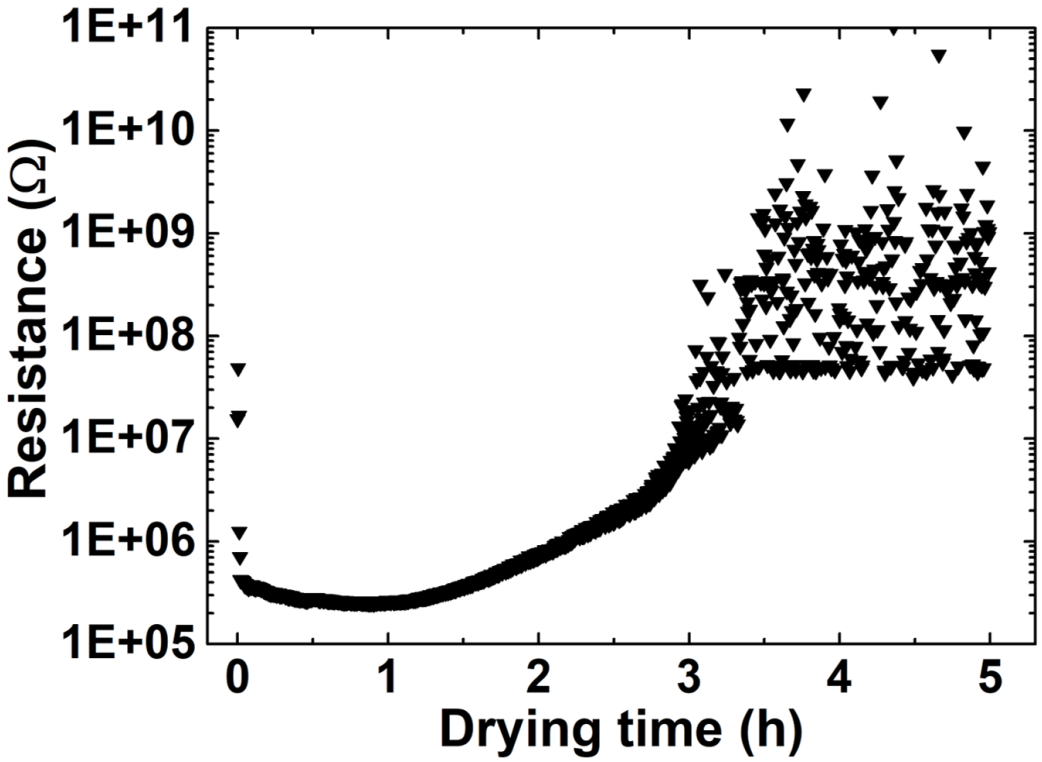

Figure S4. Resistance of t-ZnO template during infiltration with deionized water and the following evaporation of the solvent. Please note that the strong scattering of the data points after ~ 3 h results from increased noise in the high-resistance regime, which cannot be accurately detected by the Keithley sourcemeter.

Figure S5

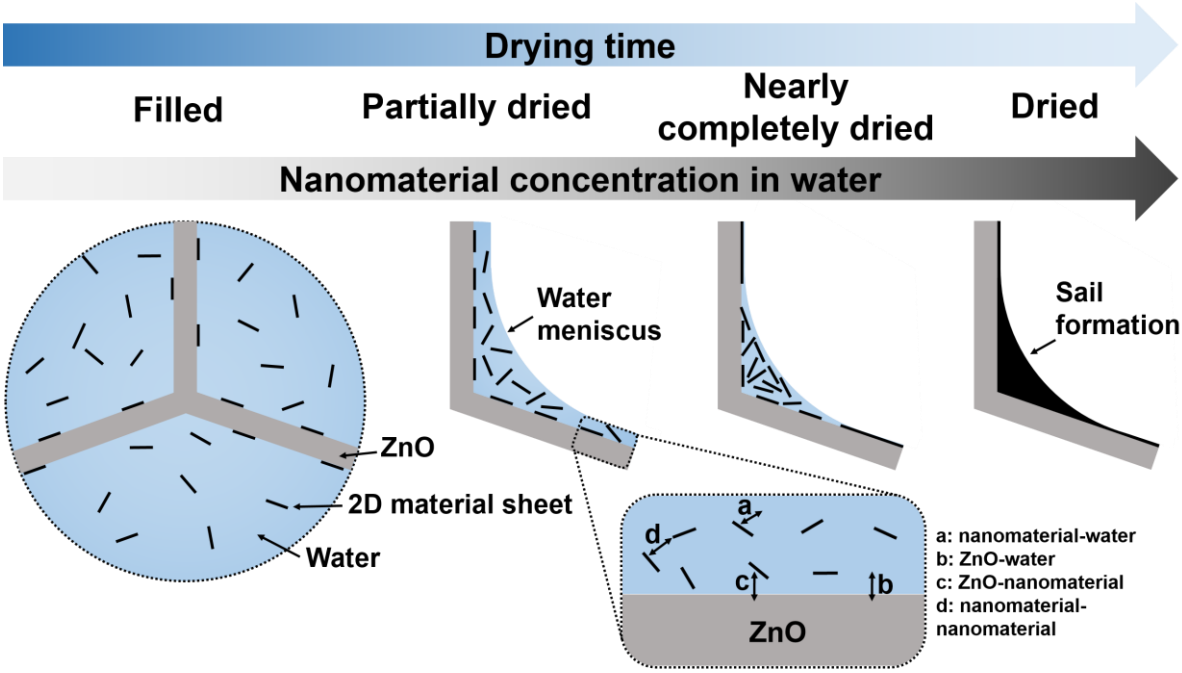

Figure S5. Assembly process of 2D carbon nanomaterials: Schematic 2D drawing of ZnO microrods after infiltration with an aqueous dispersion of nanomaterial sheets, showing four states (filled, partially dried, nearly completely dried, dried) of the subsequent proposed assembly process on ZnO.

Figure S6

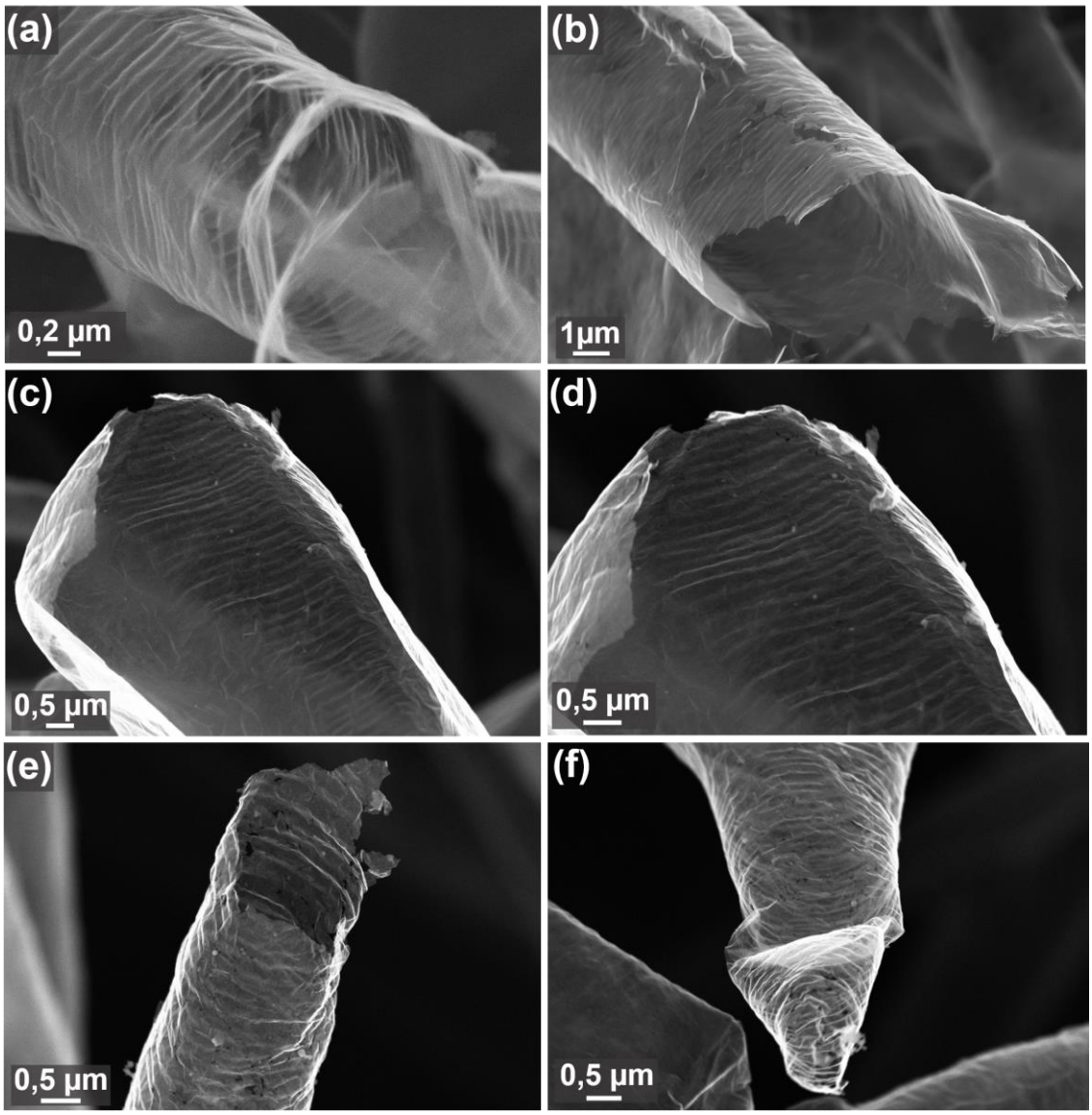

Figure S6. Adaption of template surface topography: a)-f) SEM images of **a)-b)** Aero-EG and **c)-f)** Aero-rGO, revealing corrugated surface of the hollow microtubes. These surface features arise from the ripples on the ZnO tetrapods, confirming highly conformant assembly of the carbon nanomaterials on the template.

Figure S7

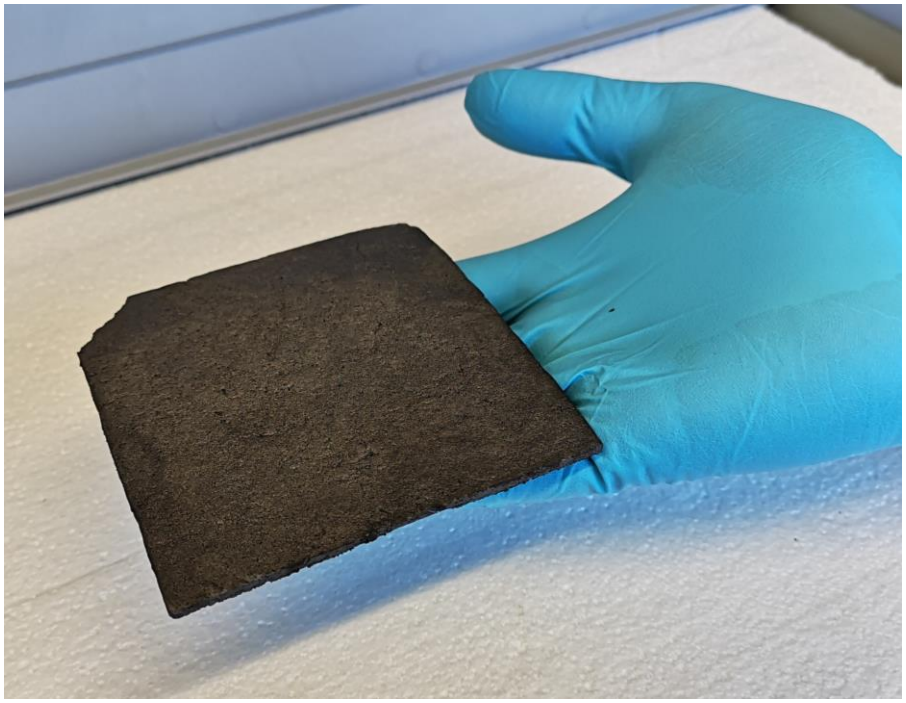

Figure S7. Photograph of a macroscopic and highly porous (> 99%) Aero-rGO sample.

Figure S8

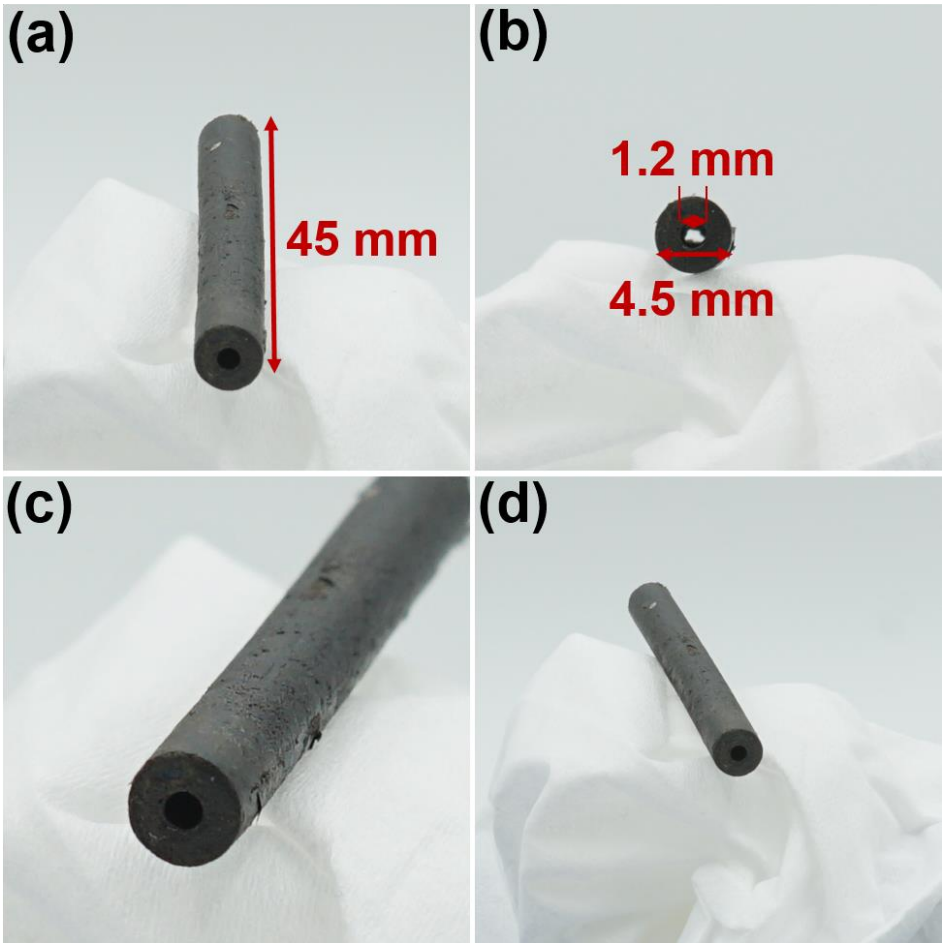

Figure S8. Macroscopic aeromaterials with complex shape: a)-d) Photographs of macroscopic Aero-GO (16 mg cm^{-3}) sample, adopting the shape of a hollow cylinder with large aspect ratio.

Figure S9

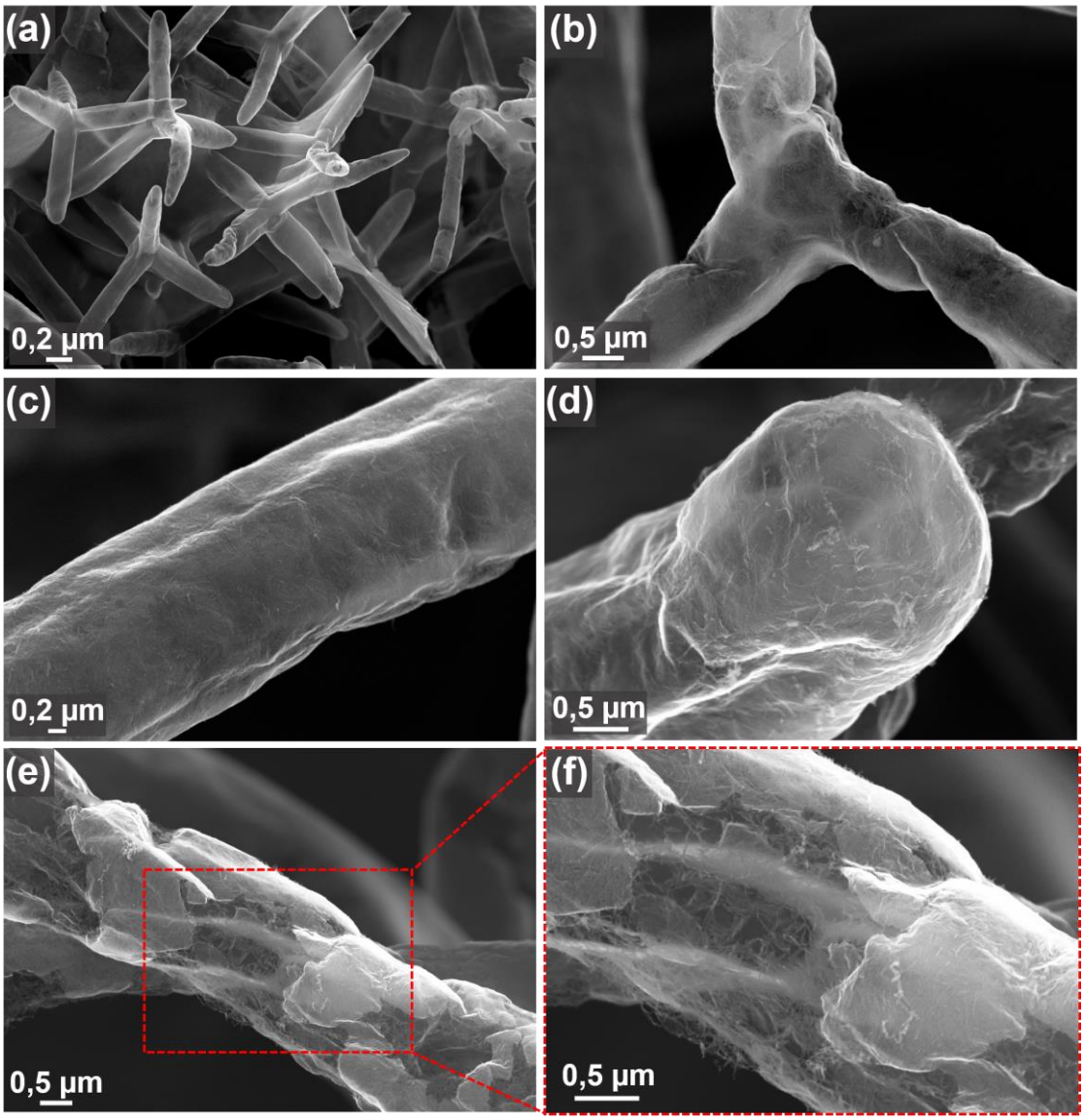

Figure S9. Combination of nanomaterials: a)-f) SEM images of Aero-rGO-CNC (cellulose nanocrystals) composites fabricated by wet-chemical infiltration of a ZnO template with an aqueous dispersion of graphene oxide (GO) flakes and CNC followed by chemical reduction of GO and template removal. The resulting tubular network is composed of a homogeneously interwoven layer of rGO flakes and CNC.

Figure S10

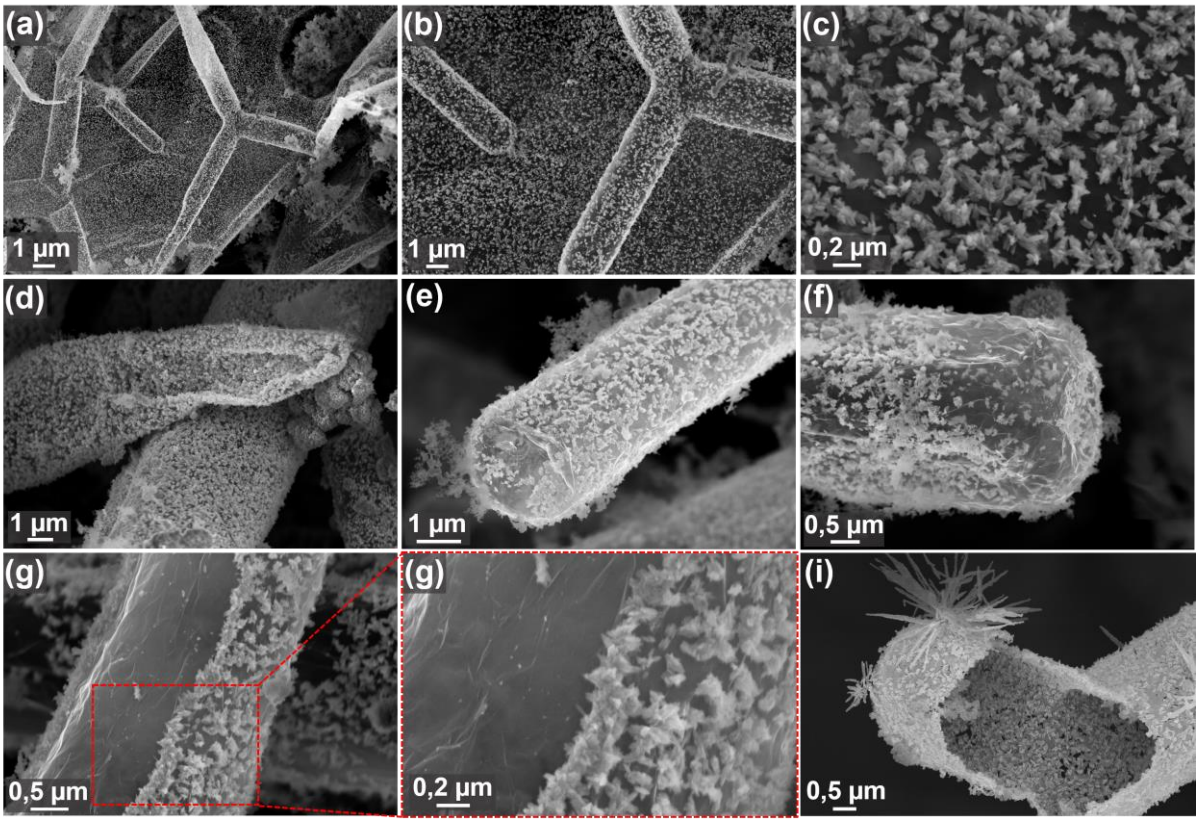

Figure S10. Functionalization of Aero-GO with $CoFe_2O_4$ nanoparticles: a)-i) SEM images of Aero-GO after functionalization with magnetic $CoFe_2O_4$ nanoparticles. Due to the ultra-low density, high specific surface area and high coverage, the macroscopic sample can be moved with a magnet (**Video S2**, Supporting Information).

Figure S11

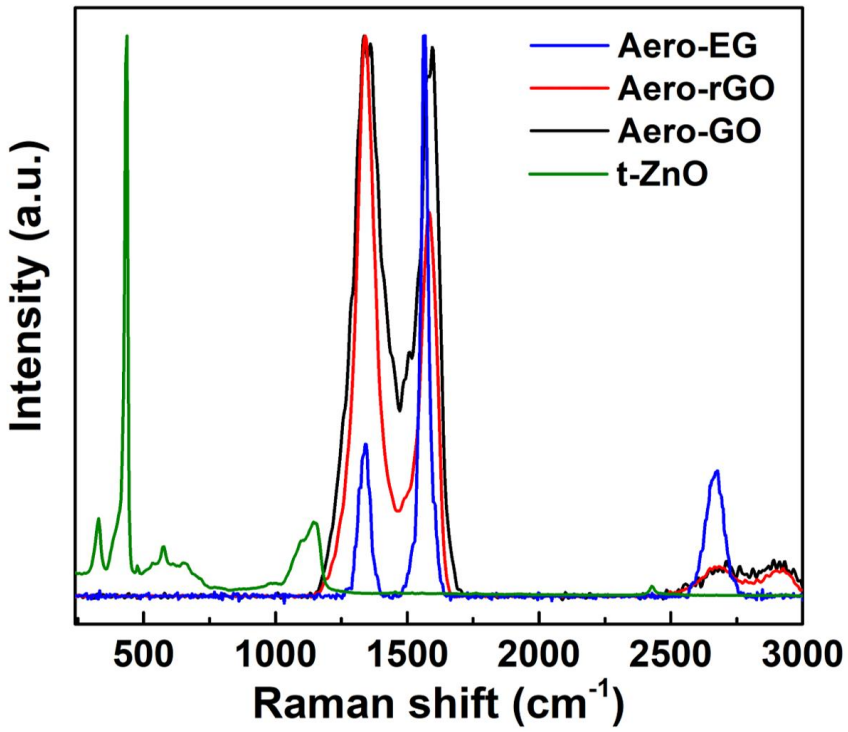

Figure S11. Raman spectra of the used t-ZnO template and the fabricated aero-networks.

Table S1. List of wet-chemically prepared graphene-polymer composites and their electric properties (from **Figure 6**). Adapted from ref.[1]

Polymer matrix	Filler	Preparation method	Filler concentration (vol.%)	Conductivity (S m^{-1})	Reference
ABS	rGO	Coagulation blending	1	0.01	[2]
Epoxy	Aerogel	Mixing	0.15	10	[3]
Epoxy	rGO	Vacuum infiltration	0.28	1	[4]
Epoxy	rGO	Casting	0.57	0.01	[5]
Epoxy	rGO	Solution blending	0.7	10^{-6}	[6]
Epoxy	Graphene nanoplatelets	Three-roll mill	0.8	7×10^{-6}	[7]
Epoxy	rGO	Solvent-free mixing	1.15	10^{-6}	[8]
Epoxy	Graphene nanoplatelets	Solution blending	1.8	10^{-6}	[9]
Epoxy	Graphene nanoplatelets	Solution blending	1	10^{-4}	[10]
Epoxy	Graphene nanoplatelets	Solution blending	1.73	10^{-4}	[11]
Epoxy	Graphene nanoplatelets	LbL assembly	2.25	10^{-4}	[12]
Epoxy	rGO	Solution blending	3	10^{-4}	[12]
Epoxy	Graphene nanoplatelets	Sonication	7.19	10^{-4}	[13]
Epoxy	Aerogel	Solution mixing	4	10^{-3}	[14]
Epoxy	Graphene nanoplatelets	Solution blending	1.73	0.01	[15]
Epoxy	rGO	*In situ* polymerization	1.15	1	[16]
HDPE	Graphene nanoplatelets	Solution blending	0.83	1.85	[17]
Hydrogel	Aerogel	*In situ* polymerization	0.23	10	[18]
NR	rGO	Coagulation blending	1.28	10^{-4}	[19]
NR	Graphene nanoplatelets	Self-assembly	5	1	[20]
PA6	Graphene	Hot compression	0.6	1	[21]
PA6	rGO	*In situ* polymerization	1.64	0.028	[22]
PA11	Graphene nanoplatelets	Masterbatch extrusion	2.68	5.2×10^{-6}	[23]

PC	rGO	Melt compounding	6.92	0.1	[24]
PCL	rGO	Solution blending	5	0.1	[25]
PE	Graphene nanoplatelets	Melt mixing	2.28	10^{-3}	[26]
PI	rGO	*In situ* polymerization	0.0075	0.32	[27]
PI	Graphene nanoplatelets	*In situ* polymerization	1.3	10^{-3}	[28]
PLA	Graphene	Solution blending	0.09	1	[29]
iPP	rGO	Melt compounding	6.92	0.01	[24]
PMMA	rGO	Self-assembly	2.6	1.2	[30]
PMMA	Graphene nanoplatelets	Solution blending	2.5	10	[31]
P(MMA-co-BA)	Graphene nanoplatelets	Latex blending	6	217	[32]
PS	rGO	Self-assembly	10^{-4}	0.15	[33]
PS	rGO	LbL assembly	0.4	0.05	[34]
PS	rGO	Solution mixing	0.86	15	[35]
PS	Graphene nanoplatelets	Solution blending	1.1	3.49	[36]
PS	Graphene nanoplatelets	Electrostatic self-assembly	1.22	25	[37]
PS	Graphene nanoplatelets	Electrostatic self-assembly	1.53	46	[38]
PS	Graphene nanoplatelets	Solution blending	4.19	13.8	[39]
TPU/PP	rGO	Melt mixing	0.82	10^{-6}	[40]

Figure S12

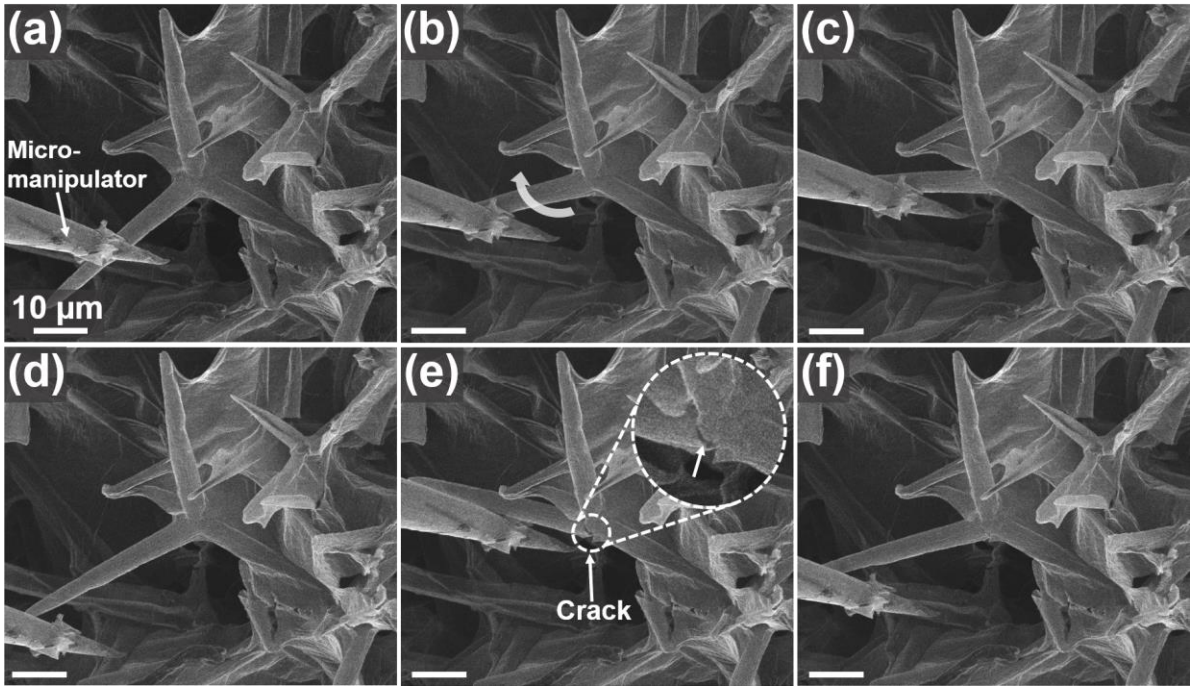

Figure S12. Reversible buckling at central joint: Sequence of SEM images showing *in situ* **a)-d)** reversible buckling of a hollow rGO microtube at central joint induced by a micromanipulator and **e)-f)** the formation of a crack at the central joint after several deformation cycles.

Figure S13

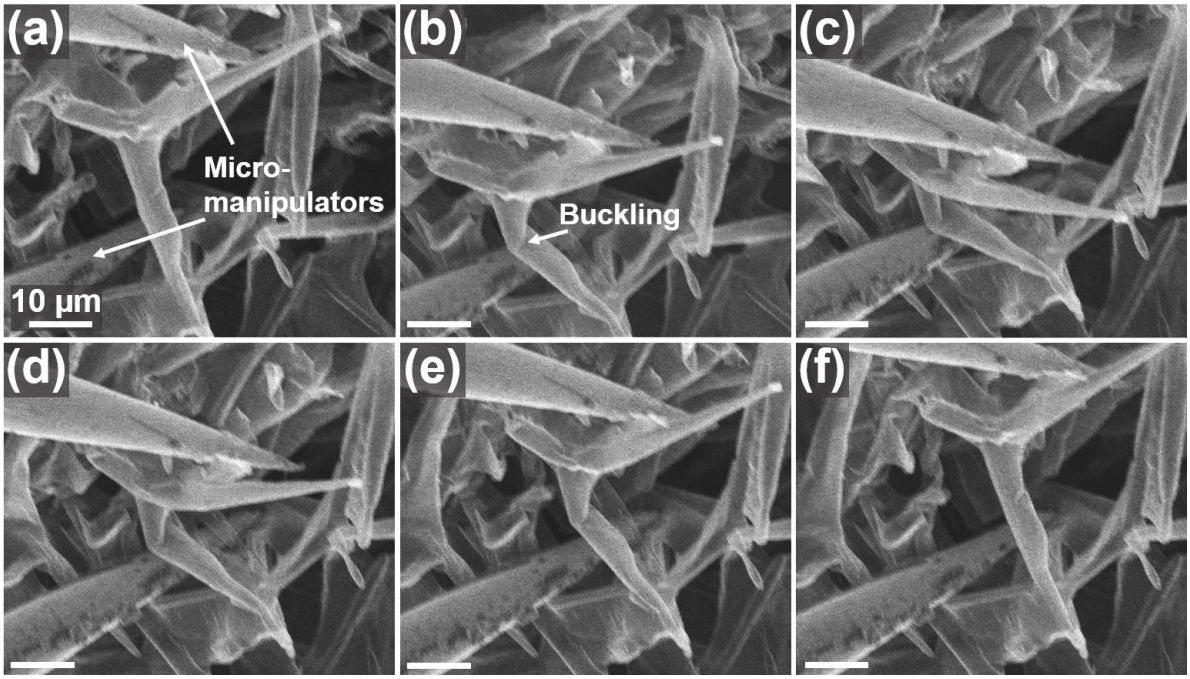

Figure S13. Reversible buckling of hollow tube: Sequence of SEM images showing *in situ* **a)-c)** buckling of a hollow rGO microtube induced by two micromanipulators, followed by **d)-f)** elastic recovery to its original shape.

Figure S14

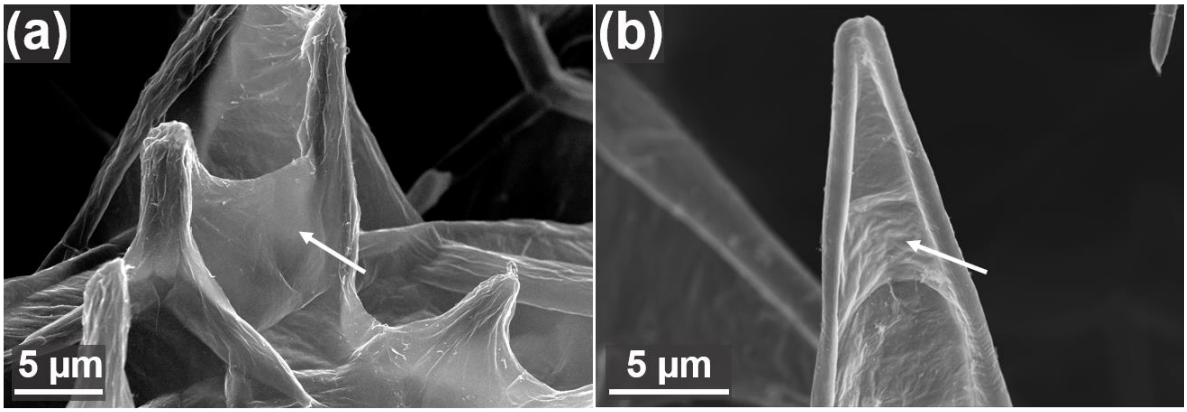

Figure S14. Nanosails: a)-b) SEM images of Aero-rGO (~ 10 mg cm^{-3}) showing nanosails between the rGO tubes, most likely arising from the wet-chemical assembly process of the GO sheets and more frequently observed with increasing density of the aeromaterials.

Supplementary Discussion

Template-Mediated Assembly of 2D Nanomaterials

The wet-chemical infiltration process is illustrated in **Figure S5**, showing four stages during drying and associated assembly of the nanomaterials on the ZnO surface. As proposed, four different interactions (a-d, Figure S5) between the solvent (water), nanomaterial sheet, and ZnO govern this process. Firstly, the combination of the interactions a (nanomaterial-water) and d (nanomaterial-nanomaterial) must allow for a stable dispersion of the nanomaterial sheets in the water without the formation of any agglomerates. Secondly, the open porosity (up to 98%) as well as the super hydrophilicity of the t-ZnO template (ZnO-water interaction) are crucial for the wet-chemical infiltration process, since they enable infiltration of the nanomaterial dispersion into the entire free volume of the network without any significant filtering effect. As demonstrated in Video S1 (showing the infiltration starting at the top side of the template), the water-based nanomaterial dispersion is soaked into the network and moves further down with each infiltrated droplet. After completed infiltration (filled state in Figure S5), the entire sample appears in a homogenous brown color (typical for the used GO dispersion) without any color gradient from top to bottom of the sample, already indicating a uniform concentration of nanomaterial sheets within the macroscopic network. This is highly important in order to ensure homogeneous coating during the subsequent assembly process. As illustrated in Figure S5, the nanomaterial concentration in the water increases with progressing evaporation of water. Due to the hydrophilic nature of ZnO, water menisci form along interconnected ZnO tetrapod arms at some point (partially dried state in Figure S5) in order to spread on the surface and minimize the interfacial energy. At the same time, the distance between the nanomaterial sheets and the ZnO tetrapod arms decreases, resulting in increased ZnO-nanomaterial interaction. With ongoing water evaporation, more sheets start to attach to the ZnO microrods and assemble on the surface to form a uniform coating. As discussed in the main manuscript, the driving force for adsorption of the nanomaterials on ZnO must be higher than the driving force for adsorption

on already deposited nanomaterials in order to achieve a homogeneous coating. It is known that ZnO intrinsically has oxygen vacancies on the surface[41,42] which are positively charged. Thus, one strategy to increase the interaction between ZnO and the nanomaterials could be the incorporation of functional groups at the edges or basal planes of the nanomaterial sheets in order to enhance the interaction. In fact, the used nanomaterials in this work (GO and EG) exhibit a significant amount of oxygen-containing functional groups which might be important for an increased interaction with ZnO and, thus, lead to a more uniform assembly on the template surface. In addition to the ZnO-nanomaterial interactions, the relatively strong interactions between the individual nanomaterial sheets are also remarkable and were revealed in the long-term compression cycling tests. Furthermore, the mechanical stability was also not compromised during the wet-chemical fabrication steps. In particular, the etching process in diluted HCl (~ 24 hours), subsequent washing in H_2O and storage of the aeromaterials in ethanol for several days did not lead to any disintegration of the structures. This is very important in view of possible applications in the field of electrochemical energy storage which often involves the use of liquid electrolytes (e.g. H_2SO_4). In this regard, the high chemical inertness of graphene and resistance toward acids represents another big advantage regarding its applicability in electrochemical applications like supercapacitors or batteries.

Eventually, the drying process can also lead to spanning of nanomaterial-assembled "sails" along interconnected ZnO microrods, arising from the high graphene concentration in the remaining water menisci. For instance, SEM images of nanosails formed in an Aero-rGO sample are presented in **Figure S14**.

References

(1) Marsden, A. J.; Papageorgiou, D. G.; Vallés, C.; Liscio, A.; Palermo, V.; Bissett, M. A.; Young, R. J.; Kinloch, I. A. Electrical Percolation in Graphene–polymer Composites. *2D Mater.* **2018**, *5* (3), 032003. https://doi.org/10.1088/2053-1583/aac055.

(2) Gao, C.; Zhang, S.; Wang, F.; Wen, B.; Han, C.; Ding, Y.; Yang, M. Graphene Networks with Low Percolation Threshold in ABS Nanocomposites: Selective Localization and Electrical and Rheological Properties. *ACS Appl. Mater. Interfaces* **2014**, *6* (15), 12252–12260. https://doi.org/10.1021/am501843s.

(3) Li, X.-H.; Li, X.; Liao, K.-N.; Min, P.; Liu, T.; Dasari, A.; Yu, Z.-Z. Thermally Annealed Anisotropic Graphene Aerogels and Their Electrically Conductive Epoxy Composites with Excellent Electromagnetic Interference Shielding Efficiencies. *ACS Appl. Mater. Interfaces* **2016**, *8* (48), 33230–33239. https://doi.org/10.1021/acsami.6b12295.

(4) Wang, Z.; Shen, X.; Akbari Garakani, M.; Lin, X.; Wu, Y.; Liu, X.; Sun, X.; Kim, J.-K. Graphene Aerogel/Epoxy Composites with Exceptional Anisotropic Structure and Properties. *ACS Appl. Mater. Interfaces* **2015**, *7* (9), 5538–5549. https://doi.org/10.1021/acsami.5b00146.

(5) Yousefi, N.; Sun, X.; Lin, X.; Shen, X.; Jia, J.; Zhang, B.; Tang, B.; Chan, M.; Kim, J.-K. Highly Aligned Graphene/Polymer Nanocomposites with Excellent Dielectric Properties for High-Performance Electromagnetic Interference Shielding. *Adv. Mater.* **2014**, *26* (31), 5480–5487. https://doi.org/10.1002/adma.201305293.

(6) Li, Y.; Tang, J.; Huang, L.; Wang, Y.; Liu, J.; Ge, X.; Tjong, S. C.; Li, R. K. Y.; Belfiore, L. A. Facile Preparation, Characterization and Performance of Noncovalently Functionalized Graphene/Epoxy Nanocomposites with Poly(Sodium 4-Styrenesulfonate). *Compos. Part A Appl. Sci. Manuf.* **2015**, *68*, 1–9. https://doi.org/10.1016/J.COMPOSITESA.2014.09.016.

(7) Wu, S.; Ladani, R. B.; Zhang, J.; Bafekrpour, E.; Ghorbani, K.; Mouritz, A. P.; Kinloch, A. J.; Wang, C. H. Aligning Multilayer Graphene Flakes with an External Electric Field to Improve Multifunctional Properties of Epoxy Nanocomposites. *Carbon N. Y.* **2015**, *94*, 607–618. https://doi.org/10.1016/J.CARBON.2015.07.026.

(8) Tschoppe, K.; Beckert, F.; Beckert, M.; Mülhaupt, R. Thermally Reduced Graphite Oxide and Mechanochemically Functionalized Graphene as Functional Fillers for Epoxy Nanocomposites. *Macromol. Mater. Eng.* **2015**, *300* (2), 140–152. https://doi.org/10.1002/mame.201400245.

(9) Zha, J.-W.; Zhang, B.; Li, R. K. Y.; Dang, Z.-M. High-Performance Strain Sensors Based on Functionalized Graphene Nanoplates for Damage Monitoring. *Compos. Sci. Technol.* **2016**, *123*, 32–38. https://doi.org/10.1016/J.COMPSCITECH.2015.11.028.

(10) Zhao, S.; Chang, H.; Chen, S.; Cui, J.; Yan, Y. High-Performance and Multifunctional Epoxy Composites Filled with Epoxide-Functionalized Graphene. *Eur. Polym. J.* **2016**, *84*, 300–312. https://doi.org/10.1016/J.EURPOLYMJ.2016.09.036.

(11) Monti, M.; Rallini, M.; Puglia, D.; Peponi, L.; Torre, L.; Kenny, J. M. Morphology and Electrical Properties of Graphene–epoxy Nanocomposites Obtained by Different Solvent Assisted Processing Methods. *Compos. Part A Appl. Sci. Manuf.* **2013**, *46*, 166–172. https://doi.org/10.1016/J.COMPOSITESA.2012.11.005.

(12) Meng, Q.; Wu, H.; Zhao, Z.; Araby, S.; Lu, S.; Ma, J. Free-Standing, Flexible, Electrically Conductive Epoxy/Graphene Composite Films. *Compos. Part A Appl. Sci. Manuf.* **2017**, *92*, 42–50. https://doi.org/10.1016/J.COMPOSITESA.2016.10.028.

(13) Moriche, R.; Sánchez, M.; Jiménez-Suárez, A.; Prolongo, S. G.; Ureña, A. Electrically Conductive Functionalized-GNP/Epoxy Based Composites: From Nanocomposite to Multiscale Glass Fibre Composite Material. *Compos. Part B Eng.* **2016**, *98*, 49–55. https://doi.org/10.1016/J.COMPOSITESB.2016.04.081.

(14) Tang, G.; Jiang, Z.-G.; Li, X.; Zhang, H.-B.; Dasari, A.; Yu, Z.-Z. Three Dimensional Graphene Aerogels and Their Electrically Conductive Composites. *Carbon N. Y.* **2014**, *77*, 592–599. https://doi.org/10.1016/J.CARBON.2014.05.063.

(15) Li, Y.; Zhang, H.; Porwal, H.; Huang, Z.; Bilotti, E.; Peijs, T. Mechanical, Electrical and Thermal Properties of in-Situ Exfoliated Graphene/Epoxy Nanocomposites. *Compos. Part A Appl. Sci. Manuf.* **2017**, *95*, 229–236. https://doi.org/10.1016/J.COMPOSITESA.2017.01.007.

(16) Yousefi, N.; Lin, X.; Zheng, Q.; Shen, X.; Pothnis, J. R.; Jia, J.; Zussman, E.; Kim, J.-K. Simultaneous in Situ Reduction, Self-Alignment and Covalent Bonding in Graphene Oxide/Epoxy Composites. *Carbon N. Y.* **2013**, *59*, 406–417. https://doi.org/10.1016/J.CARBON.2013.03.034.

(17) Castelaín, M.; Martínez, G.; Marco, C.; Ellis, G.; Salavagione, H. J. Effect of Click-Chemistry Approaches for Graphene Modification on the Electrical, Thermal, and Mechanical Properties of Polyethylene/Graphene Nanocomposites. *Macromolecules* **2013**, *46* (22), 8980–8987. https://doi.org/10.1021/ma401606d.

(18) Qiu, L.; Liu, D.; Wang, Y.; Cheng, C.; Zhou, K.; Ding, J.; Truong, V.-T.; Li, D. Mechanically Robust, Electrically Conductive and Stimuli-Responsive Binary Network Hydrogels Enabled by Superelastic Graphene Aerogels. *Adv. Mater.* **2014**, *26* (20), 3333–3337. https://doi.org/10.1002/adma.201305359.

(19) Potts, J. R.; Shankar, O.; Du, L.; Ruoff, R. S. Processing–Morphology–Property Relationships and Composite Theory Analysis of Reduced Graphene Oxide/Natural Rubber Nanocomposites. *Macromolecules* **2012**, *45* (15), 6045–6055. https://doi.org/10.1021/ma300706k.

(20) Zhan, Y.; Lavorgna, M.; Buonocore, G.; Xia, H. Enhancing Electrical Conductivity of Rubber Composites by Constructing Interconnected Network of Self-Assembled Graphene with Latex Mixing. *J. Mater. Chem.* **2012**, *22* (21), 10464. https://doi.org/10.1039/c2jm31293j.

(21) Wang, P.; Chong, H.; Zhang, J.; Lu, H. Constructing 3D Graphene Networks in Polymer Composites for Significantly Improved Electrical and Mechanical Properties. *ACS Appl. Mater. Interfaces* **2017**, *9* (26), 22006–22017. https://doi.org/10.1021/acsami.7b07328.

(22) Zheng, D.; Tang, G.; Zhang, H.-B.; Yu, Z.-Z.; Yavari, F.; Koratkar, N.; Lim, S.-H.; Lee, M.-W. In Situ Thermal Reduction of Graphene Oxide for High Electrical Conductivity and Low Percolation Threshold in Polyamide 6 Nanocomposites. *Compos. Sci. Technol.* **2012**, *72* (2), 284–289. https://doi.org/10.1016/J.COMPSCITECH.2011.11.014.

(23) Rashmi, B. J.; Prashantha, K.; Lacrampe, M.-F.; Krawczak, P. Scalable Production of Multifunctional Bio-Based Polyamide 11/Graphene Nanocomposites by Melt Extrusion Processes Via Masterbatch Approach. *Adv. Polym. Technol.* **2018**, *37* (4), 1067–1075. https://doi.org/10.1002/adv.21757.

(24) Steurer, P.; Wissert, R.; Thomann, R.; Mülhaupt, R. Functionalized Graphenes and Thermoplastic Nanocomposites Based upon Expanded Graphite Oxide. *Macromol. Rapid Commun.* **2009**, *30* (4–5), 316–327. https://doi.org/10.1002/marc.200800754.

(25) Nezakati, T.; Tan, A.; Seifalian, A. M. Enhancing the Electrical Conductivity of a Hybrid POSS–PCL/Graphene Nanocomposite Polymer. *J. Colloid Interface Sci.* **2014**, *435*, 145–155. https://doi.org/10.1016/J.JCIS.2014.08.020.

(26) Tu, C.; Nagata, K.; Yan, S. Influence of Melt-Mixing Processing Sequence on Electrical Conductivity of Polyethylene/Polypropylene Blends Filled with Graphene. *Polym. Bull.* **2017**, *74* (4), 1237–1252. https://doi.org/10.1007/s00289-016-1774-4.

(27) Park, O.-K.; Kim, S.-G.; You, N.-H.; Ku, B.-C.; Hui, D.; Lee, J. H. Synthesis and Properties of Iodo Functionalized Graphene Oxide/Polyimide Nanocomposites. *Compos. Part B Eng.* **2014**, *56*, 365–371. https://doi.org/10.1016/J.COMPOSITESB.2013.08.065.

(28) Park, O.-K.; Hwang, J.-Y.; Goh, M.; Lee, J. H.; Ku, B.-C.; You, N.-H. Mechanically Strong and Multifunctional Polyimide Nanocomposites Using Amimophenyl Functionalized Graphene Nanosheets. *Macromolecules* **2013**, *46* (9), 3505–3511. https://doi.org/10.1021/ma400185j.

(29) Sabzi, M.; Jiang, L.; Liu, F.; Ghasemi, I.; Atai, M. Graphene Nanoplatelets as Poly(Lactic Acid) Modifier: Linear Rheological Behavior and Electrical Conductivity. *J. Mater. Chem. A* **2013**, *1* (28), 8253. https://doi.org/10.1039/c3ta11021d.

(30) Vo, N. H.; Dao, T. D.; Jeong, H. M. Electrically Conductive Graphene/Poly(Methyl Methacrylate) Composites with Ultra-Low Percolation Threshold by Electrostatic Self-Assembly in Aqueous Medium. *Macromol. Chem. Phys.* **2015**, *216* (7), 770–782. https://doi.org/10.1002/macp.201400560.

(31) Mutlay, İ.; Tudoran, L. B. Percolation Behavior of Electrically Conductive Graphene Nanoplatelets/Polymer Nanocomposites: Theory and Experiment. *Fullerenes, Nanotub. Carbon Nanostructures* **2014**, *22* (5), 413–433. https://doi.org/10.1080/1536383X.2012.684186.

(32) Noël, A.; Faucheu, J.; Rieu, M.; Viricelle, J.-P.; Bourgeat-Lami, E. Tunable Architecture for Flexible and Highly Conductive Graphene–polymer Composites. *Compos. Sci. Technol.* **2014**, *95*, 82–88. https://doi.org/10.1016/J.COMPSCITECH.2014.02.013.

(33) Wu, C.; Huang, X.; Wang, G.; Lv, L.; Chen, G.; Li, G.; Jiang, P. Highly Conductive Nanocomposites with Three-Dimensional, Compactly Interconnected Graphene Networks via a Self-Assembly Process. *Adv. Funct. Mater.* **2013**, *23* (4), 506–513.

https://doi.org/10.1002/adfm.201201231.

(34) Fan, W.; Zhang, C.; Tjiu, W. W.; Liu, T. Fabrication of Electrically Conductive Graphene/Polystyrene Composites via a Combination of Latex and Layer-by-Layer Assembly Approaches. *J. Mater. Res.* **2013**, *28* (04), 611–619. https://doi.org/10.1557/jmr.2012.437.

(35) Tkalya, E.; Ghislandi, M.; Alekseev, A.; Koning, C.; Loos, J. Latex-Based Concept for the Preparation of Graphene-Based Polymer Nanocomposites. *J. Mater. Chem.* **2010**, *20* (15), 3035. https://doi.org/10.1039/b922604d.

(36) Qi, X.-Y.; Yan, D.; Jiang, Z.; Cao, Y.-K.; Yu, Z.-Z.; Yavari, F.; Koratkar, N. Enhanced Electrical Conductivity in Polystyrene Nanocomposites at Ultra-Low Graphene Content. *ACS Appl. Mater. Interfaces* **2011**, *3* (8), 3130–3133. https://doi.org/10.1021/am200628c.

(37) Zhao, P.; Luo, Y.; Yang, J.; He, D.; Kong, L.; Zheng, P.; Yang, Q. Electrically Conductive Graphene-Filled Polymer Composites with Well Organized Three-Dimensional Microstructure. *Mater. Lett.* **2014**, *121*, 74–77. https://doi.org/10.1016/J.MATLET.2014.01.100.

(38) Tu, Z.; Wang, J.; Yu, C.; Xiao, H.; Jiang, T.; Yang, Y.; Shi, D.; Mai, Y.-W.; Li, R. K. Y. A Facile Approach for Preparation of Polystyrene/Graphene Nanocomposites with Ultra-Low Percolation Threshold through an Electrostatic Assembly Process. *Compos. Sci. Technol.* **2016**, *134*, 49–56. https://doi.org/10.1016/J.COMPSCITECH.2016.08.003.

(39) Liu, N.; Luo, F.; Wu, H.; Liu, Y.; Zhang, C.; Chen, J. One-Step Ionic-Liquid-Assisted Electrochemical Synthesis of Ionic-Liquid-Functionalized Graphene Sheets Directly from Graphite. *Adv. Funct. Mater.* **2008**, *18* (10), 1518–1525. https://doi.org/10.1002/adfm.200700797.

(40) Lan, Y.; Liu, H.; Cao, X.; Zhao, S.; Dai, K.; Yan, X.; Zheng, G.; Liu, C.; Shen, C.; Guo, Z. Electrically Conductive Thermoplastic Polyurethane/Polypropylene Nanocomposites with Selectively Distributed Graphene. *Polymer (Guildf).* **2016**, *97*, 11–19. https://doi.org/10.1016/J.POLYMER.2016.05.017.

(41) Mishra, Y. K.; Kaps, S.; Schuchardt, A.; Paulowicz, I.; Jin, X.; Gedamu, D.; Freitag, S.; Claus, M.; Wille, S.; Kovalev, A.; et al. Fabrication of Macroscopically Flexible and Highly Porous 3D Semiconductor Networks from Interpenetrating Nanostructures

by a Simple Flame Transport Approach. *Part. Part. Syst. Charact.* **2013**, *30* (9), 775–783. https://doi.org/10.1002/ppsc.201300197.

(42) Gedamu, D.; Paulowicz, I.; Kaps, S.; Lupan, O.; Wille, S.; Haidarschin, G.; Mishra, Y. K.; Adelung, R. Rapid Fabrication Technique for Interpenetrated ZnO Nanotetrapod Networks for Fast UV Sensors. *Adv. Mater.* **2014**, *26* (10), 1541–1550. https://doi.org/10.1002/adma.201304363.